Geophysical Journal International

Geophys. J. Int. (2012) **188,** 908–924 doi: 10.1111/j.1365-246X.2011.05300.x

High-resolution magnetotelluric studies of the Archaean–Proterozoic border zone in the Fennoscandian Shield, Finland

K. Vaittinen,[1] T. Korja,[1] P. Kaikkonen,[1] I. Lahti[2] and M. Yu. Smirnov[1]

[1]*Department of Physics, Geophysics Group, University of Oulu, Oulu, Finland. E-mail: katri.vaittinen@oulu.fi*
[2]*Bedrock Geology and Resources, Geological Survey of Finland, Rovaniemi, Finland*

Accepted 2011 October 26. Received 2011 July 30; in original form 2010 November 10

SUMMARY

The Archaean–Proterozoic collisional zone is a complex mixture of the Archaean complexes [e.g. Iisalmi Complex (IC)], Proterozoic supracrustal belts [e.g. Kainuu Belt (KB) and Savo Belt (SB)] and oceanic arc lithologies in the central Fennoscandian Shield. The zone was formed in the Savo orogeny when the Keitele microcontinent collided with the Archaean Karelian craton in the Palaeoproterozoic time. The crustal architecture of this palaeosuture is studied using new broad-band magnetotelluric data from 104 sites. 2-D conductivity models across the border zone between the Palaeoproterozoic Svecofennian Domain and the Archaean Karelian province are constrained using the recent, partly collocated reflection seismic data from the Finnish Reflection Experiment (FIRE). Dimensionality analyses, in particular the *Q*-function analysis, show that magnetotelluric data represent reasonably well regional 2-D structure at periods <100 s, which is the longest period used in this study. Strike determinations gave a stable strike of N15W. For the inversions, the data are projected into three parallel profiles with an azimuth of N75E. The determinant inversion is selected as the most suitable method for the data set. Especially the phase data are useable only from the determinant since one of the polarizations have the out-of-quadrant phase at several sites. The interpreted final, geological more appropriate models, where smoother thick conductive areas are replaced by thinner layers, are constructed from the results of the unconstrained smooth inversions with the help of forward modelling, synthetic and prior model inversions and reflection seismic models. The two major sets of crustal conductors are identified. They have an opposite dip and together they form a bowl-shaped conductor. In the west, the eastward dipping SB conductors are located at the bottom of the formation underlain by the Keitele microcontinent. The SB conductors extend to the east possibly cutting the westward dipping conductors of the KB. The conductive KB is flanked above and below by the resistive Archaean IC/Rautavaara and Eastern Finland Complexes and represents the remnants of a basin that was squeezed between two Archaean blocks in the collision. The crustal conductors revealed by the inversion extend to the surface, where they can be associated with the near-surface conductors mapped by airborne electromagnetic surveys. Geological mapping has shown that the near-surface conductors are caused by graphite and/or sulphide-bearing metasedimentary rocks. Thus the deep conductors related with the Proterozoic KB and SB were formed on the surface and transported into the upper and middle crustal levels in the Savo orogeny. The crust in the Karelian Craton is highly resistive having only minor resistivity variations in our research area. Also the Archaean lower crust is resistive on the contrary to the conductive lower crust of the Proterozoic SB and the Keitele microcontinent.

Key words: Electrical properties; Magnetotelluric; Cratons; Crustal structure; Europe.

1 INTRODUCTION

The magnetotelluric (MT) method uses the Earth's electromagnetic (EM) field as the source for investigating the subsurface electrical resistivity structure (Tikhonov 1950; Cagniard 1953). Detailed description of the theoretical background of the method and models can be found, for example, in Berdichevsky & Dmitriev (2009). The combination of MT and reflection seismic methods has repeatedly proven to be effective in crustal studies because these two methods provide independent data sets and therefore complement each

other. Magnetotellurics is more sensitive to the texture and conductive fillings of the subsurface rather than volume (Hjelt *et al.* 2006) and, in addition to conductivity models, also provides information on the dimensionality and orientation of the structures (Korja & Hjelt 1998). Consequently models, built in particular on reflection seismic data, can be tested by MT method, and vice versa (Jones 1998). Encouraged by this, the MT-FIRE project has acquired high-resolution MT data around the Finnish Reflection Experiment (FIRE, e.g. Kukkonen *et al.* 2006) profiles and along the older deep seismic sounding line SVEKA (Luosto *et al.* 1984).

Results from our profiles in the surroundings of the FIRE-1 transect in eastern Finland (Fig. 1) are presented in this paper.

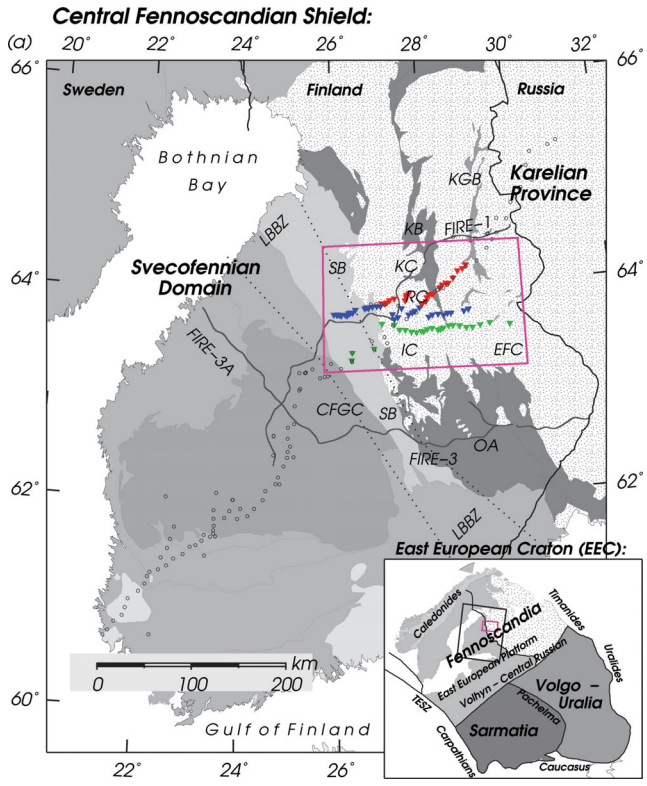

Figure 1. Geological and geophysical maps of the study area. (a) Geological map of the Central Fennoscandian Shield (modified from Koistinen *et al.* 2001). The study area is marked with a purple box. FIRE-1, FIRE-3 and FIRE-3A profiles are shown with thick black lines. Abbreviations: CFGC, Central Finland Granitoid Complex; EFC, Eastern Finland Complex; IC, Iisalmi Complex; KB, Kainuu Belt; KC, Kajaani Complex; KGB, Kuhmo Greenstone Belt; LBBZ, Lake Ladoga – Bothnian Bay zone; OA, Outokumpu Area; RC, Rautavaara Complex; SB, Savo Belt. (b) Location of the MT-FIRE magnetotelluric (MT) soundings and the lithology of the research area (modified from Koistinen *et al.* 2001). MT sites are shown as circles. Filled circles denote sites used in 2-D analysis; red for profile P1, blue for P2 and green for P3. Open circles are sites omitted from 2-D analyses and open circles with cross are sites of poor data quality. The common midpoints of the reflection seismic FIRE-1 profile form a thick blue line. (c) Apparent resistivity map of the study area. Map shows the near-surface resistivity obtained from airborne electromagnetic surveys (Peltoniemi *et al.* 1990; Airo 2005) by calculating apparent resistivities from real and imaginary data using the approach of Pirttijärvi (1995). Only resistivities lower than 200 Ωm are shown with different shades of red. MT sites from SVEKA (Korja & Koivukoski 1994) and GGT/SVEKA (Lahti *et al.* 2002) projects are shown as yellow diamonds. MT-FIRE sites and FIRE-1 profile are shown as in (b). Scalar audiomagnetotelluric SVEKA profile (Kaikkonen & Pajunpää 1984) is shown with a dashed black line. Shotpoints of deep seismic sounding line SVEKA (Luosto *et al.* 1984) are shown with stars.

The seismic transect crosses the boundary zone between the Archaean Karelian and Palaeoproterozoic Svecofennian parts of the Fennoscandian Shield. At the surface this palaeosuture features a mixture of Archaean complexes [e.g. Iisalmi complex (IC)], Proterozoic supracrustal belts [e.g. Kainuu Belt (KB) and Savo Belt (SB)] and oceanic arc lithologies. Our data cover primarily the palaeosuture zone but extend to the Archaean Karelian domain in the east.

Properties, structure and evolution of ancient continent–continent collisions help us to understand properties and dynamics of modern and ongoing processes because the ancient zones reveal the final structure produced by collisions and usually also the properties of deeper crustal sections. The structure of the Proterozoic continent–continent collisional zone in the Central Fennoscandian Shield was investigated.

Ancient continent–continent collisional zones (palaeosutures) often contain metasedimentary rocks with interconnected conducting phases, for example, graphite, sulphides and iron oxides (e.g. Duba *et al.* 1994), which are effectively imaged by EM methods. Large-scale crustal conductors can be studied best by magnetovariational (MV) arrays and MT profiles whereas the mapping of the near-surface conductivity structures requires methods having denser lateral coverage such as airborne electromagnetic (AEM) measurements made in the area by the Geological Survey of Finland (Airo 2005). The combination of these different data sets provides us a powerful tool that allows us to investigate in detail both the position of conductors with respect to geological and tectonic structures and the internal structure of the conductors themselves (Korja & Hjelt 1998).

Broad-band MT data from several profiles are used to study the architecture of the crust at the Karelian–Svecofennian collisional zone and in the Karelian Craton far from the collisional zone. Primary aims are to define (1) the geometry and properties of the subduction-related structures between the Karelian Craton and the primitive island arc complex, (2) the role of the Archaean IC and Proterozoic KB in collision, (3) the continuation of the KB conductor to the south, that is, to examine if there is an unexposed connection between the KB in north and the Outokumpu Area in south suggesting that they form a single sedimentary basin and (4) the internal structure of the highly resistive Karelian craton.

2 AREA OF INTEREST: GEOLOGICAL BACKGROUND AND GEOPHYSICS

2.1 Geological background

The East European Craton (EEC) consists of the Fennoscandian, Sarmatian and Volgo-Uralian crustal segments. The northern and central parts of the Fennoscandian segment are known as the Fennoscandian Shield, which is further divided into the Archaean Karelian, Belomorian and Kola provinces, the Proterozoic Svecofennian Domain (Orogen), and the Southwest Scandinavian Domain (Gaál & Gorbatschev 1987; Fig. 1 litological map after Koistinen *et al.* 2001). Overview of the geological evolution of the research area in the Fennoscandian Shield is given in Table 1. In the west, the Shield is flanked by the Palaeozoic Caledonian Orogen. This study concentrates on the boundary zone between the Archaean and Proterozoic crustal units, the major tectonic boundary (Ar-Pt boundary) in the Shield. The study covers also the western part the Archaean Karelian province in the east. The upper crustal units along our profiles, approximately from northeast to southwest, are:

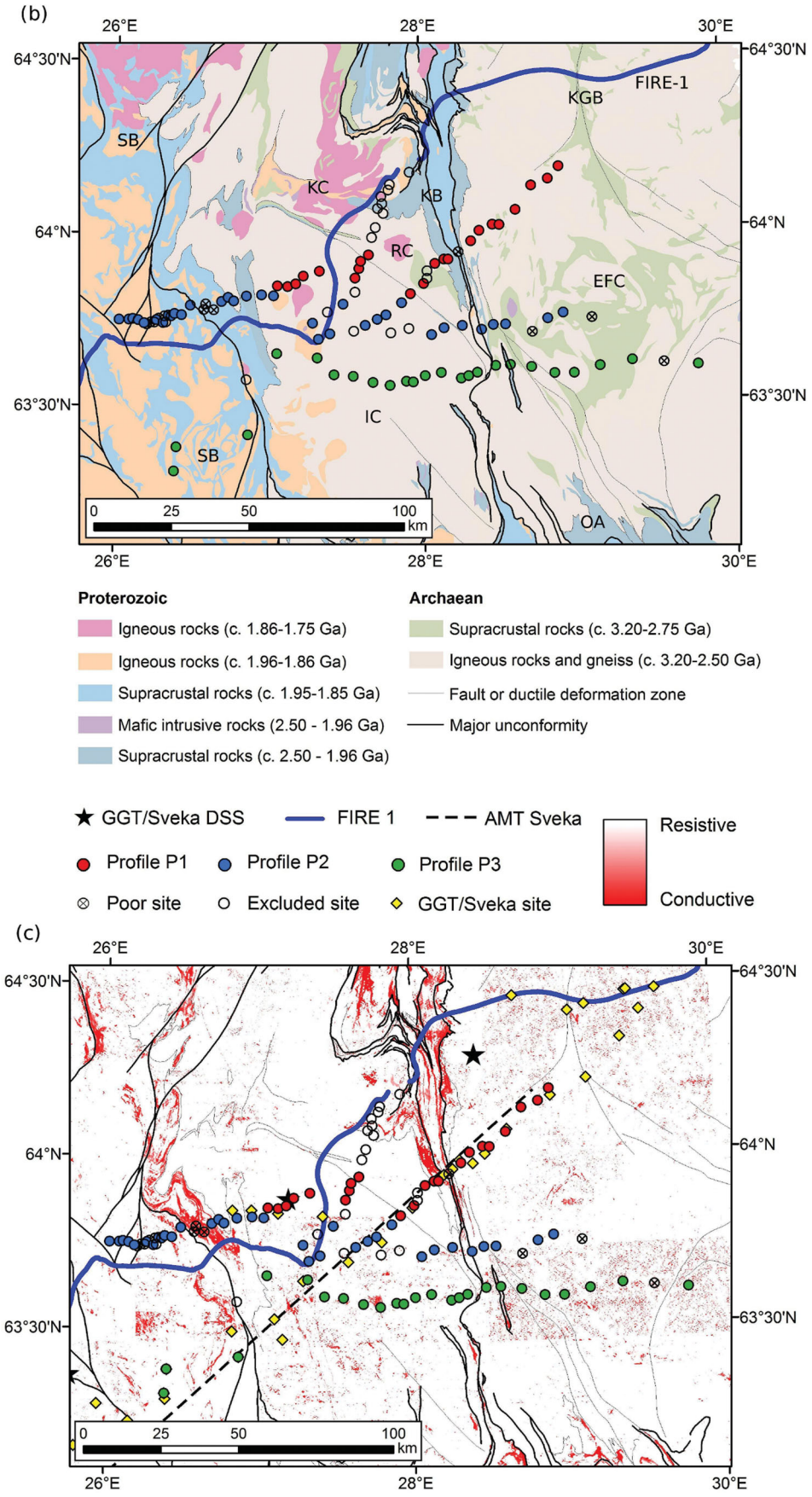

Figure 1. (*Continued.*)

Table 1. Geological evolution of the Central Fennoscandian Shield.

Age (Ga)	Orogeny	Description
3.1–2.9	Saamian	Formation of the Karelian province: a granite-greenstone terrain (rifted crust) with N–S and NNE–SSW aligned greenstone belts
2.9–2.6	Lopian	
2.5–1.97		Craton partially covered with sediments and volcanic rocks
		Rifting, break-up and opening of a sea; passive margin
1.93–1.91	Lapland-Kola	Karelian craton forms a stable nucleus for the Fennoscandian Shield in subsequent orogenies[a]
1.92–1.76	Svecofennian	
	Svecofennian[b]	
1.92–1.88		Microcontinent accretion:
	Lapland-Savo	Accretion of the Norrbotten, Keitele and Bothnian microcontinents to the Karelian craton
	Fennian	Subsequent accretion of the Bergslagen microcontinent
1.87–1.84		Stabilization by extension:
		Large-scale extensional basins filled with psammites and pelites[c] Mafic dyke and granite intrusions[d,e]
1.87–1.79		Continent–continent collisions:
1.84–1.81		Collision of the Fennoscandia and Kola cratons (Laurentia) in the northeast
1.83–1.80		Docking of Sarmatia in the southeast
1.84–1.80	Svecobaltic	Unknown continent docking in the southwestern margin
1.82–1.80	Nordic	Collision of the Fennoscandian and Amazonian continents in the west
1.79 and 1.77		Stabilization period:
		Gravitational collapse, thermal resetting and late tectono-magmatic episodes

[a]Gorbatschev & Bogdanova (1993).
[b]Korja *et al*. (2006).
[c]Lahtinen *et al.* (2002).
[d]Stålhös (1976).
[e]Suominen (1991).

Eastern Finland Complex (EFC), KB, IC, Kajaani Complex (KC) and Rautavaara Complex (RC) and SB (Nironen *et al.* 2002).

The Neoarchaean EFC is composed of migmatic tonalites and trondhjemites. Intrusions of granites and granodiorites are also present as well as Archaean supracrustal banded amphibolites (Luukkonen 2001). The EFC is further divided into the Eastern and Western Kianta Blocks, which are separated by the Kuhmo Greenstone Belt.

The KB is a Palaeoproterozoic metasedimentary cover between the EFC and the IC and KC. It is composed of allochthonous pelitic and turbiditic sequences. The eastern segment of the KB consists of turbidites but in the western segment also ophiolites are present (Kontinen & Meriläinen 1993).

The KC to the northwest of the KB is rather heterogenous formation with Archaean granitoids and Proterozoic para-autochthonous cover sequences of quartzite, dolomite, metadolorite and volcanic rocks (Korsman *et al*. 1997). The RC to the south of the KC is dominated by approximately 2.8–2.7 Ga Archaean migmatites. Further to the southwest lies the IC, which consists mainly of 3.2–3.1 Ga Archaean tonalitic–trondhjemitic migmatites, amphibolites and granulites. Several steeply dipping and NW–SE striking Proterozoic diabases are also found in the IC, contrary to the RC, which is characterized by the rareness of such dykes. The same NW–SE strike is also common direction for faults and fracture zones in the area (Paavola 1990, 1999).

The Archaean–Proterozoic suture is marked at the surface by the eastern edge of the SB. The SB (1.96–1.85 Ga) consists of SE–NW trending metavolcanic and metaturbiditic rocks interlayered with gneissic tonalites (Lahtinen 1994). Central Finland Granitoid Complex consists mainly of synkinematic granitoids and granodiorites, which have been later intruded by post-kinematic granitoids, granodiorites, quarz monzonites and gabbros (Nironen 2003). Remnants of volcanic and metasedimentary supracrustal belts are also abundant in the area.

2.2 Previous EM and seismic work

Fennoscandian crust is generally very resistive and contains prominent elongated conductors (Pajunpää 1987). The deep conductivity anomalies delineate the boundaries between, for example, the Archaean and Proterozoic crustal units and are interpreted to represent closed basins between older crustal blocks (Korja *et al*. 1993; Korja 1993; Hjelt *et al*. 2006). Some of these crustal conductors can be traced up to the surface using the airborne data. The graphite- and sulphide-bearing schists of the KB are seen as very good conductors (10^{-1}–10 Ωm, Fig. 1). Another highly conductive feature is associated with the eastern border of SB, where the resistivities are several tens of ohm metres. The conductors of the Outokumpu Area are located in the southern edge of our research area (Fig. 1c).

The first deep EM work in the research area was done by Ádám *et al.* (1982). Kaikkonen & Pajunpää (1984) presented a 2-D conductivity model constructed from 1-D interpretations of 140 scalar audiomagenetotelluric (AMT) soundings (3700–8 Hz). The profile crosses the Ar-Pt boundary zone in SW–NE direction along the seismic SVEKA line (Luosto *et al.* 1984; Fig. 1c). Kaikkonen & Pajunpää (1984) identified three regions, based on different average resistivities, of which the middle one is the most conductive. They interpreted enhanced conductivities to represent either the change of rock types or fractures in the Lake Ladoga – Bothnian Bay zone (LBBZ), or both. The area was later covered by magnetometer array studies (Pajunpää 1984, 1987), which divided the Finnish part of the Fennoscandian Shield into four distinct geoelectric regions. The boundary between the very resistive eastern block (II) and more conductive middle block (I) coincides with the Kuhmo Greenstone Belt that is located in the eastern edge of our study area. Furthermore, a minor conductor was detected at the KB.

Korja & Koivukoski (1994) constructed a forward 2-D model from new broad-band tensor MT soundings (0.1–1000 s) along the entire SVEKA profile. The 16 easternmost sites of the profile

coincide with the MT-FIRE research area. The model from this part of the profile reveals a prominent SW dipping upper crustal conductor beneath the KB but does not image any conductors associated with the LBBZ probably due to the lack of short period AMT data and large site distance. They further concluded that the Karelian crust is very resistive in comparison to the Svecofennian crust in general.

Lahti *et al.* (2002, see also Hjelt *et al.* 2006) extended the old MT SVEKA profile and presented a 2-D inversion model along the GGT/SVEKA transect (Korsman *et al.* 1999). The main results for our area of interest are that the LBBZ (Ar-Pt boundary) does not exhibit major resistivity changes. The strongest regional scale conductivity boundary is between the resistive Archaean and more conductive Proterozoic lithosphere beneath the KB about 80 km NE of the suture. The KB is represented by a southwest dipping conductor extending to the depth of 20 km under the IC.

Refraction seismic studies (Luosto 1991, 1997; Korja *et al.* 1993; Korsman *et al.* 1999) suggest that in general the Archaean crust is thinner than the Proterozoic. The average crustal thickness in the Karelian province is 40 km, while the thickest crust of about 60 km is found beneath the LBBZ. Most of the variations in the Moho depth are due to variations in the high-velocity lower crust. The areas of thin crust have been subject to extensional events and the areas of thicker crust have reached isostatic balance by crustal density variations caused by magmatic intra- and underplating.

The most recent geophysical work in the area is the reflection seismic FIRE project (Kukkonen & Lahtinen 2006). The reflectivity pattern of the upper crust in the FIRE-1 profile is well correlated with surface lithological units (Korja *et al.* 2006). They interpret the upper crustal reflectivity pattern by lithological contacts or shear zones or their combination. The KB and autochthonous units at the western edge of the EFC are characterized by 30–45° westerly dipping band of reflections, which are cut by steeper (<60°) west-dipping poorly reflective zones. The gently dipping strong reflectors are correlated at surface with the greywacke-pelite association. The units of KB can be traced at least to the depth of 10 km based on the reflectivity pattern (Korja *et al.* 2006). The shallow Salahmi autochthonous cover at the western edge of IC has steep (70°) west-dipping reflectors. Based on the reflection data, this formation might be a few kilometres deep. The contact of the mica gneisses in the SB is marked by abrupt change to moderately (25–30°) west-dipping reflectors (Korja *et al.* 2006) in the upper crust. Deeper below the SB, the reflectors dip to the east. In the MT-FIRE research area, also gravimetric, magnetic, geothermal and rheological studies have been carried out as a part of the GGT/SVEKA transect compilation (Korsman *et al.* 1999) and the FIRE project (Kukkonen & Lahtinen 2006).

3 MEASUREMENTS AND DATA ANALYSIS

3.1 Measurements and time-series processing

Broad-band MT soundings were carried out at 104 sites during 2003–2005 using instruments recently developed in the University of Uppsala (Smirnov *et al.* 2008). Magnetic field was measured with induction coils from Metronix (MSF05) and electric field with two perpendicular electric dipoles (Pb-PbCl non-polarizable electrodes). Length of the dipoles varied from 50 to 100 m. The instruments are equipped with EarthData recorder, which allows acquisition at two sampling frequencies simultaneously. The 20 Hz recordings were continuous for a minimum of 1 d at each site, while the 1000 Hz was recorded for 2 hr after midnight (burst mode recording) to enhance signal-to-noise ratio with higher world thunderstorm activity and less cultural noise. The 3000 Hz data were acquired for 0.5 to 1 hr before or after the main recording phase. Concerning transfer functions, these sampling frequencies mean period range from 1/1000 s to 1000 s and even longer at sites where recordings lasted several days. Depending on the subsurface conductivity in the research area, these periods allow us to investigate the structures of the crust and upper lithospheric mantle, except for the uppermost few kilometres.

Distances between the sites vary from 1 to 5 km. High-resolution data with broad frequency range and short distances between the sites make it possible to gain a very detailed picture of the underlying earth. In comparison to the older MT measurements in the research area (Korja & Koivukoski 1994; Lahti *et al.* 2002), the new transfer functions cover almost three more decades of periods and the site distances are five–ten times shorter. Data measured in geomagnetic coordinates were rotated to geographic coordinates, using declination maps provided by the Finnish Meteorological Institute. The declination in the study area changes from 7.5° in the west to 9.5° in the east.

The site locations were selected to get a good coverage across the palaeosuture and to make 3-D modelling of the KB conductors possible in the future. To effectively correlate the results with seismic studies, some sites were located as close as possible to the FIRE and SVEKA profiles. However, since the FIRE project used the Vibroseis method, the reflection seismic profiles are located at the main roads. On the other hand, to minimize EM noise the MT sites need to be far from the roads and buildings. Therefore most of the MT sites do not coincide with position of the seismic profiles. The southernmost sites form a profile to determine if there is an unexposed connection between the conductors in KB and in the Outokumpu Area. The location of our measurements as well as the FIRE profiles is shown in Figs 1(a) and (b), and the location of older MT, AMT and seismic work with the near-surface conductivity map in Fig. 1(c).

The data were processed using the robust multiremote reference code by Smirnov (2003). It is based on robust statistics that have been shown to be very efficient against outliers. The data recorded at 3000 Hz data were subject to single site (SS) processing only as no remote reference (RR) recordings were available in this mode. Most of the sites were recorded in RR mode, which improves the quality of transfer functions. The distances between the local and remote site were usually not less than 20 km, which proved to be enough to improve the data quality. The most significant improvement of RR processing over SS in the frequency was noted in the range from 1 to 100 Hz. Different Fourier transform lengths were examined during processing. Usually 3–10 different Fourier windows, whose lengths ranged from 32 to 26 2144 samples, were used for each three sampling frequencies (20 Hz, 100 Hz and 3000 Hz). The final transfer functions are averages over all individual estimates. Only six sites out of the initial 104 were rejected due to very low quality of the final transfer functions, caused by severe local EM noise.

The transfer functions are very consistent with gradual variations from site to site and they share common regional features. Overall quality of the transfer functions is excellent and their strange behaviour at some sites is most likely due to complexity of the geoelectric structure rather than any measuring or processing errors. For example, at sites on top of the RC, the determinant impedance phases are abnormally high reaching and even exceeding 90° after 10 s (Fig. 2, 'bad' sites). At these sites, there is also a large split

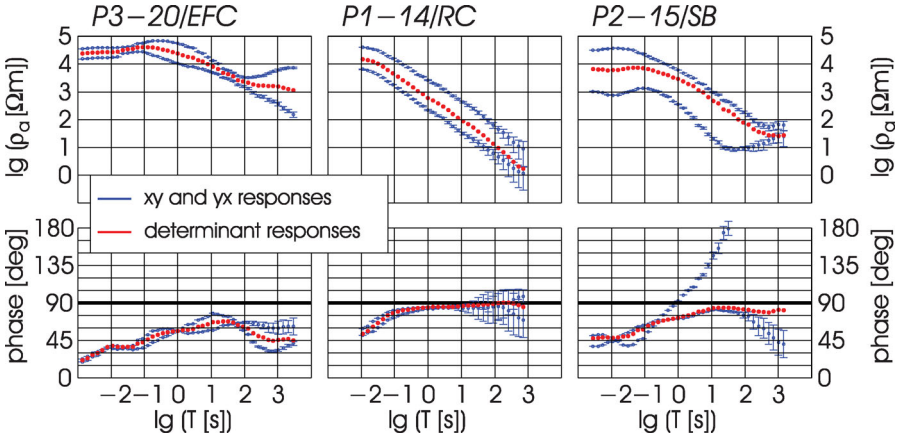

Figure 2. Examples of observed data from three characteristic sites, the good (left), the bad (middle) and the ugly (right). Apparent resistivities from all tensor components and determinant average are shown in upper panel and phases from off-diagonal tensor components and the determinant average in lower panel. Vertical bars denote real confidence limits. Responses are shown in the coordinate system rotated to the strike of –15°. Blue curves are *xy*- and *yx*-responses and red curves determinant averages. Data from sites P3–20 (20th site from west on profile P3) and P2–15 represent typical sites measured in the Eastern Finland Complex and the Savo Belt (Fig. 1), respectively. The site P3–20 represents a 'good' site for all 2-D inversions, not only for the determinant. P2–15 is an example of an 'ugly' site, where one of the polarizations cannot be used in 2-D inversion, but the determinant inversion is possible. Data from site P1–14, which is measured on the Kainuu Belt–Rautavaara Complex boundary, represents 'bad' sites where even the determinant phases exceed 90° at long periods. These are the sites where periods longer than 10 s had to be excluded from 2-D inversion.

between *xy*- and *yx*-phases, where one of the polarizations goes out of quadrant and the apparent resistivity curve resembles a line descending in a 45° angle as would be the case for so called perfect conductor. In addition at most of the sites in the SB area either *xy*- or *yx*-phase is out of quadrant, but usually the determinant phase remains below 90° and is consistent with determinant apparent resistivity (Fig. 2, 'ugly' sites). At some sites cultural noise (e.g. electrical fences) or instrument malfunction (fuses burnt by lightning) caused failures in electric field measurements so that only tipper data are available. Also at a few sites, the vertical magnetic field was not measured.

Based on the extreme behaviour of the phases as explained above 12 sites and, at five sites on top of RC, the periods longer than 10 s were excluded from further analyses and inversion. For final analyses and inversion the accepted sites were divided into three roughly east–west directed profiles: P1 in the north (24 sites), P2 (34 sites) in the middle and P3 (23 sites) in the south (Fig. 1). From 88 sites suitable for 2-D analyses nine sites were excluded from this study because of their long distance to the selected profiles. The remaining 79 sites are used to analyse dimensionality and strike properties of the area as well as to perform 2-D inversions along the selected profiles.

Induction arrows (Parkinson 1962; Wiese 1962) are a graphical presentation of the magnetic transfer function (tipper). They generally identify the direction and magnitude of conductivity changes. In the study area, they are generally rather small: at periods from 1 to 100 s, 80 per cent are below 0.3 (Fig. 3). The anomalous induction arrows (>0.3) from this study and from the older data set (Pajunpää 1984, 1987) are shown in Fig. 3. Periods selected from MT-FIRE data are 1 s, 10 s and 100 s (from blue to green) and from the old data 100 s, 300 s and 1000 s (from green to yellow). The directions of the arrows for the selected data set are stable except for two locations at the period of 1 s. On contrary, the directions of arrows shorter than 0.3 and at periods smaller than 1 s, vary greatly indicating local induction effects. The selected thresholds leave a reasonable amount of tipper data for inversion only in the eastern part of the profile P1 (KB, Fig. 9). The selected tipper data are also used in the strike analysis (Fig. 5).

3.2 Dimensionality and strike analyses

The MT transfer functions allow the investigation of the dimensionality and directional properties of the subsurface in the research area. The knowledge of the dimensionality of the area ensures selection of proper tools (1-D, 2-D and 3-D) to invert and interpret the data. In the case of 2-D earth, the strike direction must be found to decompose impedance tensor into E and H polarizations. It is also important to project the measured sites to a profile perpendicular to the strike to get a correct geometry of the model even if the inversion of a rotational invariant such as determinant is used.

The skew of the impedance tensor is a measure of dimensionality. In general, the larger the skew values are, the more the underlying structures deviates from one or two dimensions. Bahr (1988) suggested regional skews which take into account near-surface 3-D distortions in otherwise 1-D or 2-D earth. According to Bahr's (1988) recommendation, the regional 1-D indicator (3-D/1-D skew) should be below 0.1 for regional 1-D structure and below 0.3 for regional 2-D structure. Note, however, that this condition is necessary but not adequate, that is, there might be cases (see, e.g. Ledo *et al.* 2002) where 3-D structures produce skews <0.3. In our area, the 3-D/1-D skew is always higher than 0.2. The 3-D/2-D skews (shown in Fig. 4) are generally below the limit of the 2-D regional structure. However, in the profile P2, under the IC (21.–26. site) and the eastern part of the SB (11.–17. site), the skews are systematically higher than 0.3.

There are several ways to estimate the geoelectric strike from MT and geomagnetic depth sounding (GDS) data. The phase sensitive strike (principal superimposition model) of Bahr (1988, 1991), *Q*-function strike (Zhang *et al.* 1987; Smirnov & Pedersen 2009) and the induction arrows are used in this study. The Bahr strike is defined for underlying 2-D regional structure in the presence of 3-D near-surface inhomogenities. In the *Q*-function analysis the strike direction is found by minimizing the object function (*Q*-function) as discussed by Smirnov & Pedersen (2009). The *Q*-function is the sum of normalized squared misfits between the measured diagonal elements and those predicted from the off-diagonal elements in the same column of the impedance tensor at several periods and

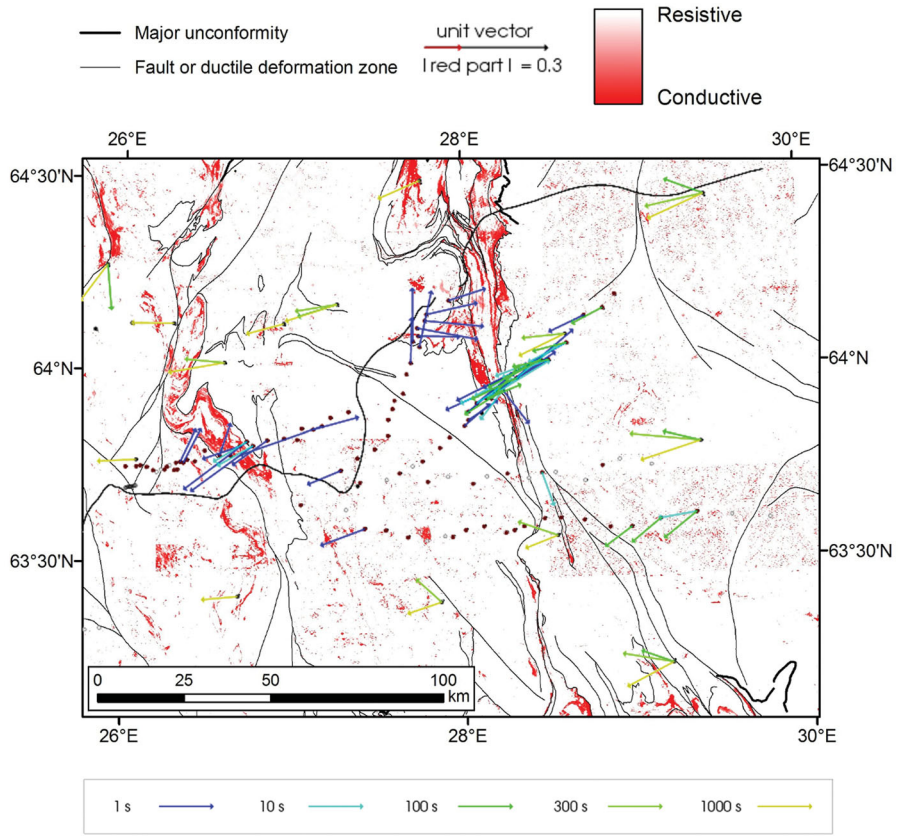

Figure 3. Reversed induction arrows (Parkinson 1962) longer than 0.3 as a function of period. Arrows drawn in blue to green are from this study and in green to yellow from earlier magnetometer array studies (Pajunpää 1984, 1987). Background as in Fig. 1(c).

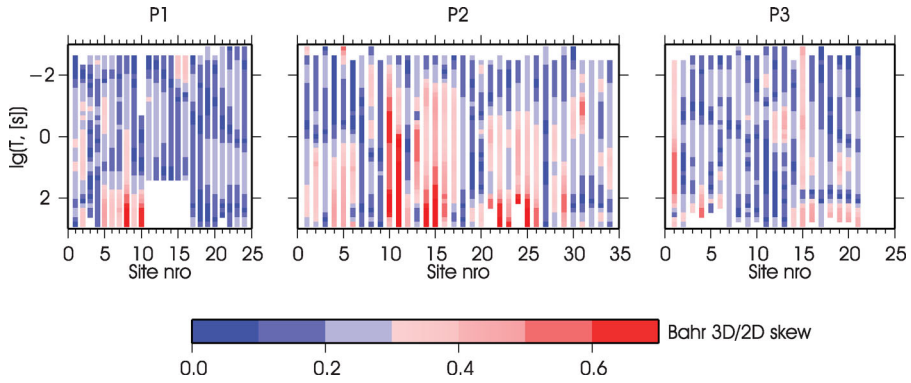

Figure 4. Bahr 3-D/2-D skew values (Bahr 1991) for profiles P1 (left panel), P2 (centre panel) and P3 (right panel). Threshold of 0.3 is marked by the change of colour from blue to red. Overall the skews are small, and the largest values are obtained at central parts of P2 beneath the Savo Belt and Iisalmi Complex.

sites. However, the direction estimated from the impedance tensor is subject to 90° ambiguity. This ambiguity can be resolved using induction arrows, which in 2-D environment are perpendicular to the geoelectric strike. In Fig. 5 the results from three different strike analyses are shown, including Bahr's (1988) regional strikes (Fig. 5 upper row), *Q*-function strikes (Fig. 5 lower row), and the strike direction determined from induction arrows (red overlay in both figures).

In the Bahr and *Q*-function analysis, strikes were calculated at seven frequencies per decade at each site to get statistically more reliable results. Yet frequencies higher than 1 Hz were omitted from the analysis, because the highest frequencies are the noisiest and they only represent the uppermost parts of the subsurface. For induction arrows one period per decade is used, starting from 1/100 s.

The strikes estimated from the induction arrows and from the impedance tensor are in a good agreement at the profiles P1 and P3, but differ at profile P2. In the profile P2, the induction arrows are not equally distributed along the whole profile (Fig. 3). In the west, the spatial sampling is denser and H_z was measured at each site, whereas in the east, the site distances are longer and H_z was measured only at every second site. Thus the statistical analysis is not very reliable in this case. The Bahr strikes for each profile are scattered over a wide range of directions while the *Q*-function strikes seem to define a more stable direction (–10° to –30°/+80° to

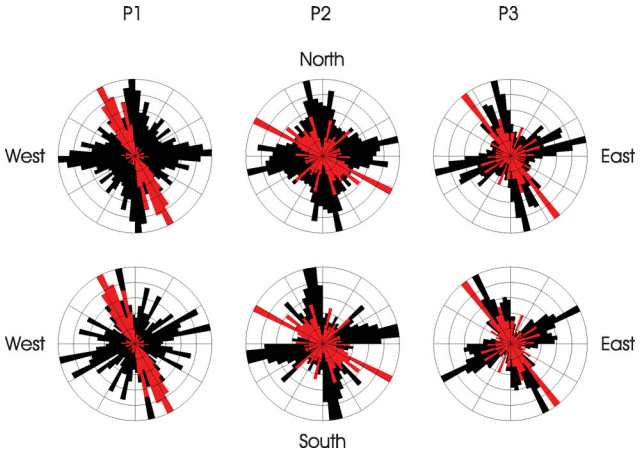

Figure 5. Rose diagrams showing the strike directions estimated from impedance tensor and induction arrows that are longer than 0.3. In the upper row, Bahr (1988) regional strikes are shown as black roses and the strike direction determined from induction arrows as red roses. In the lower row, the strike directions determined from the *Q*-function analysis (Zhang *et al.* 1987) are shown as black roses and the strikes from the induction arrows as red. The length of each class is normalized so that the length is one for the class with the most frequent strike. Since the goal is to find a regional strike direction, data at periods longer than 1 s are used in both cases. P1, P2 and P3 stand for the profiles.

+60°) probably due to better constraints. In the *Q*-function analysis the solution was obtained for averaging over three periods and three sites. The induction arrows suggest a strike direction of –10° to –30°. Thus the strike is around –20° rather than +70°. This direction is also in agreement with the large-scale surface lithological features.

Q-function analysis (Fig. 5) suggests strikes of –15° or –30° for the profile P1, –15° for profile P2 and –30° for profile P3. For P1, the strike of –30° is also supported by induction arrow directions. However, to carry out 2-D inversion the area has to be assumed to be 2-D, the same strike is selected for all profiles. To find out which of the two strikes (–15° or –30°) suggested by the *Q*-function analysis satisfy better the 3-D/2-D assumption, the *Q*-function at each site and period for both strikes was calculated (Fig. 6). The upper row shows $Q^{1/2}$-value at the strike of –15° and the lower row at –30°. Basically, the value of one means, that the impedance tensor satisfies regional 2-D assumptions while the larger values indicate deviations from it. Differences between these two strikes are not remarkable, therefore, with the same level of confidence a common strike between –15° and –30° can be chosen. Another result of this test was that it is mostly the longest periods that do not satisfy the 2-D assumption, thus it was decided to reject the periods longer than 100 s from this study. In most cases the longer periods already carry information from the mantle, while this study concentrates on crustal structures. For periods shorter than 100 s, the strike of –15° is slightly better and was used to project data for inversion.

4 INVERSION AND DISCUSSION ON MODELS OBTAINED

The traditional approach in 2-D inversion of MT data has been fitting the data in the *E*-polarization and *H*-polarization. The polarizations have been fitted either separately or jointly, without and later also with the tipper. In our case, one of the phases, either *E*- or *H*-polarization, is out-of-quadrant in several sites (Fig. 2, 'ugly' sites). This results in high skew values (>0.3, Fig. 4) and also indicates 3-D effects. Consequently the 2-D inversion of either polarization (or joint inversion of the polarizations) proved to be problematic. For example, the test inversions of TE/TM modes gave rms errors of 10–13. In comparison, rms for the final determinant models is 1.0–1.5, while for homogeneous half-space (starting model) rms is approximately 17. To improve the fit of the TE + TM inversion, several sites should have been omitted: in the profile P2, this would mean 62 per cent of all data. To significantly increase the amount of measured data usable for 2-D inversion, the phase and apparent resistivity estimated from the determinant average of the impedance tensor $\mathbf{Z}_{\mathbf{DET}} = \sqrt{Z_{xx}Z_{yy} - Z_{xy}Z_{yx}}$ (Berdichevsky & Dmitriev 1976) were used. Moreover, they demonstrated that the use of effective impedances (e.g. determinant) considerably reduces the 3-D distortions of the MT responses. Pedersen & Engels (2005) numerically compared the determinant and two polarization responses for different synthetic 3-D/2-D models, and concluded, after several inversion tests, that the $\mathbf{Z}_{\mathrm{DET}}$ response is the smoothest and more robust against 3-D effects.

The determinant is rotationally invariant, that is, the impedance data to be inverted do not depend on the strike direction at all. Thus the variations in the strike direction along the profile and as a function of the period, caused by 3-D effects, do not have that much effect on the determinant inversion results. The only aspect the strike affects in the determinant inversion is the relative site distances along the profile. In contrast to traditional approach, where the strike must be found to rotate the data to the principal coordinate system, in the determinant inversion the strike is only needed to project the profiles perpendicular to it. This ensures that the true earth geometry is preserved in the model.

Prior to inversion, the sites were projected to new profiles perpendicular to the strike (N75E). At this stage, five sites were omitted since the distances between the sites along the projected profile would have been only few hundreds of metres. Minimum of 1 km for the site distance along the profiles was used. The three profiles have respectively 23, 34 and 24 sites used in inversion with corresponding average site distances of 4.2, 4.1 and 7.2 km when the projected profile lengths are taken into account. Three sites from the GGT/SVEKA data set were added to the western end of the profile P3.

In general, data from 700 Hz to 100 s was included in the inversion. The determinant responses of this period range can be fitted with 1-D model for most of the sites. Thus the phase and apparent resistivities are consistent with each other indicating that the dispersion relations (Weidelt & Kaikkonen 1994; Berdichevsky & Pokhotelov 1997) between them are satisfied and the data quality is good. The periods longer than 100 s do not satisfy the 2-D assumption for the selected strike direction as seen in Fig. 6.

The final grid has 200 cells in the vertical direction and, depending on the profile length, 230–330 cells in the horizontal direction. The bottom of the grid is at 1500 km and 10 exponentially growing air cells are added above the ground surface. The model edges are 2300 km away from the ends of the profile. A homogenous half-space with the resistivity of 1000 Ωm is used as a starting model.

Galvanic effects may seriously distort the impedance tensor thus introducing bias in final models. Error floor weighting has typically been used to reduce this effect by assigning larger error floors to the apparent resistivity than the phase and tipper. Additionally, the inversion can create small-scale near-surface inhomogenities to compensate for static shift. The error floor was 16 per cent on the

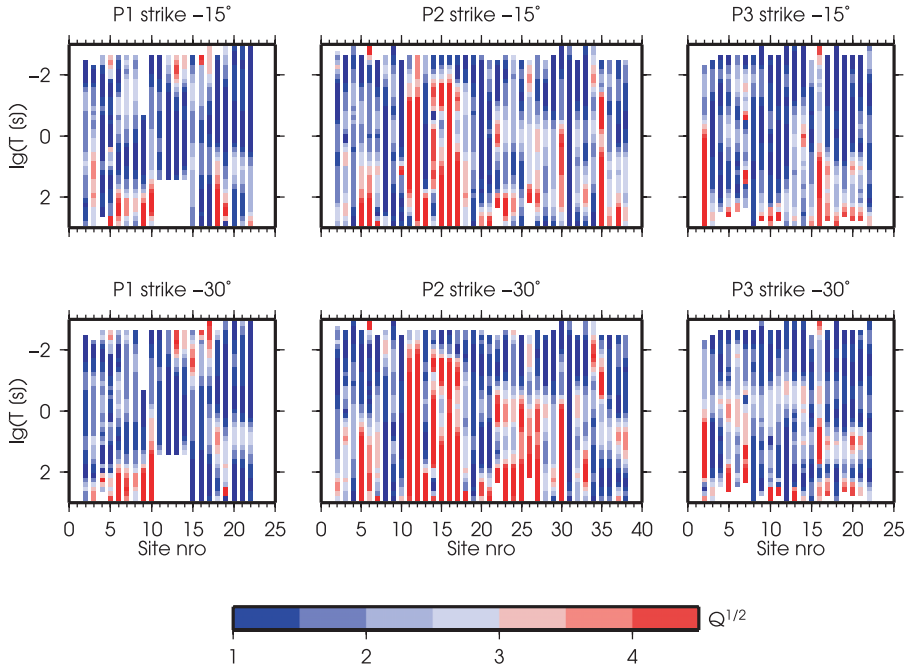

Figure 6. The $Q^{1/2}$ values calculated for the data. If $Q^{1/2}$ value equals 1 then the data satisfy the assumption of 3-D/2-D structure within the error floor of 5 per cent. The highest $Q^{1/2}$ value of 4 in this data set means that all data would fit the 3-D/2-D assumption within the error floor of 20 per cent. This can be used in inversion by increasing the error floor into this level and therefore to ensure that probable 3-D features in data are not fitted.

apparent resistivity to allow enough freedom for the inversion to overcome static distortions and to prevent most of the 3-D features to be fitted with artificial 2-D structures. On the impedance phase, the absolute error floor of 3° was used. The REBOCC code (Siripunvaraporn & Egbert 2000) modified for the determinant inversion by Pedersen & Engels (2005) was used in the inversion.

The final inversion models obtained are shown in Fig. 7. Characteristic for the entire study area is a strong contrast between the resistive and relatively homogeneous eastern part (B1, B2, B3; Archaean EFC) and generally more conducting and heterogeneous western part (complex mixture of Proterozoic and Archaean rocks). Main features in the western part are (1) westward dipping conductors A1 and A2, (2) an eastward dipping conductor E in profile P2 and its absence G in profile P3 forming another strong contrast/gradient in the models and (3) conductors D1 and D2 below resistive upper crust (C1, C2) and conductor K in the middle crust in the profile P3. Minor distinguishable features are a near-surface conductor F at profile P2, a faint conductor I at profile P3 and the conductivity changes in the lower crust and mantle in the western part of profile P3 (J) and in the eastern part of the study area (H1, H2, H3).

Comparison of observed data and model responses as well as their difference (misfit) are shown in Fig. 8. Misfits are normalized by data errors, that is, misfit of one means perfect fit within the data errors. The fit of the data is generally good. Particularly, the apparent resistivity is fitted with rms below one along the whole profile and at all periods. In the phase misfit plot, there are higher misfits, the worst of which (rms > 2) are painted black in Fig. 8 for an easy identification. In the profile P3, a few higher misfit values are found more randomly scattered along the profile, that is, there are no clearly problematic areas in P3. The worst misfits are related to the abnormally high phases, for example, in the profile P1 starting from 40 km. It seems that the inversion algorithm cannot generate models with high enough phases to fit our data. Another problem might arise from a large variation in the phase values between two neighbouring sites: as seen in the measured data (φ_{obs}), the phases rapidly change from 85–90° to 60–70° (P1 ∼55 km, P2 ∼107 km). The difference between the measured and model phases has its maximum of about 10° at these sites. Thus the final model conductivities (Fig. 7) could be slightly lower than the true conductivities. The high observed phases may also be due to 3-D effects as suggested by the *Q*-analysis (Fig. 6).

4.1 Model testing and discussion

4.1.1 Tipper tests

The conductor A is one of the most prominent features in our models, but according to model fit it is also quite a problematic area. The conductor coincides spatially with the near-surface conductivity anomalies observed by airborne measurements (Fig. 1c), which suggests that the near-surface conductors represent the exposed parts of the deep conductor. Measurement of the electric field right on the top of the near-surface conductors failed resulting in an increased MT site distance and consequently reduced model resolution near the surface. The lack of data in this critical area affected the resulting determinant model, where the top of the conductor A appears to be at the depth of 3–4 km. Since the induction arrows were also exceptionally large and stable in this area, it was possible to include them in the inversion of the profile P1 to gain some additional information on the nature of conductor A. The magnetic fields were successfully recorded at each site which added one extra tipper site for the inversion on top of A. The comparison of the models is shown in Fig. 9: the joint inversion result confirms the suggestion that the conductors detected both by the airborne and MT measurements represent the same structure.

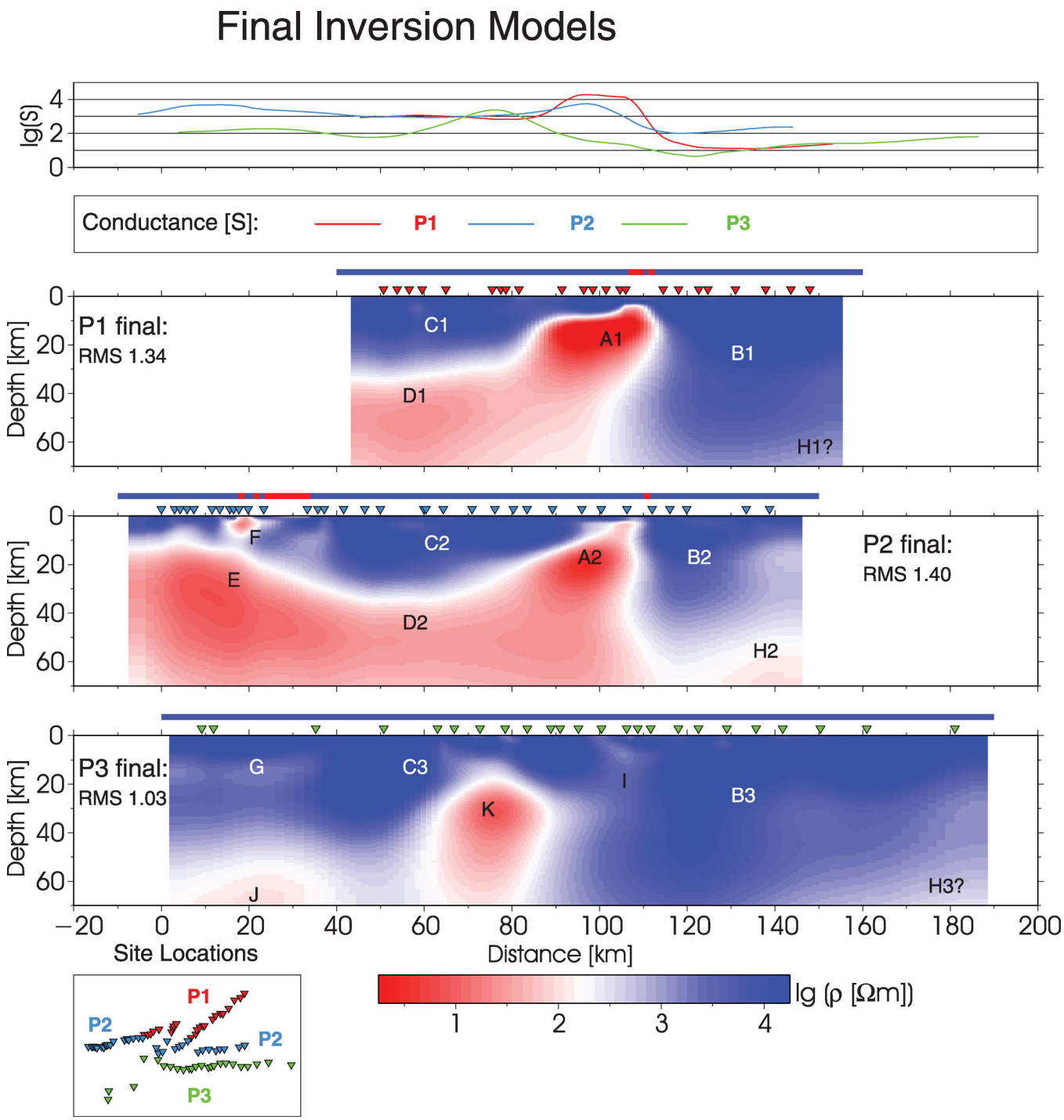

Figure 7. Final 2-D inversion models for all profiles in the direction of N75E. Models P1 and P3 are shifted to the east to preserve geographical relations between the profiles. Each mesh cell forming the model is drawn and coloured according to their resistivities. The uppermost graph shows conductance (S) values for each model integrated from the surface to the depth of 70 km. The conductance is expressed as $S = \int_{h_1}^{h_2} \sigma(z)\,\mathrm{d}z$, where $\sigma(z) = 1/\rho(z)$ (S m^{-1}) is the conductivity distribution with the depth z, ρ (Ωm) is resistivity and h_1 and h_2 are depth limits along the profile. Inverted triangles show the locations of soundings. The locations of the near-surface conductors mapped by AEM is shown by red in a thin stripe above each profile. Letters A–K mark features that will be discussed and/or interpreted. If the feature can be tracked in several profiles, also a number is assigned to it.

4.1.2 Prior/synthetic model tests

A few different prior models were used in test inversions for each profile to determine which structures are needed to fit the data and to test how stable our inversion models are. The prior model provides very strong constraints for the inversion, that is, the resulting model is obtained in the vicinity of *a priori* model. Small changes are possible to improve the rms fit, but the inversion cannot significantly change the prior model. If large changes to the chosen prior model were needed to improve the fit, the inversion would result in an

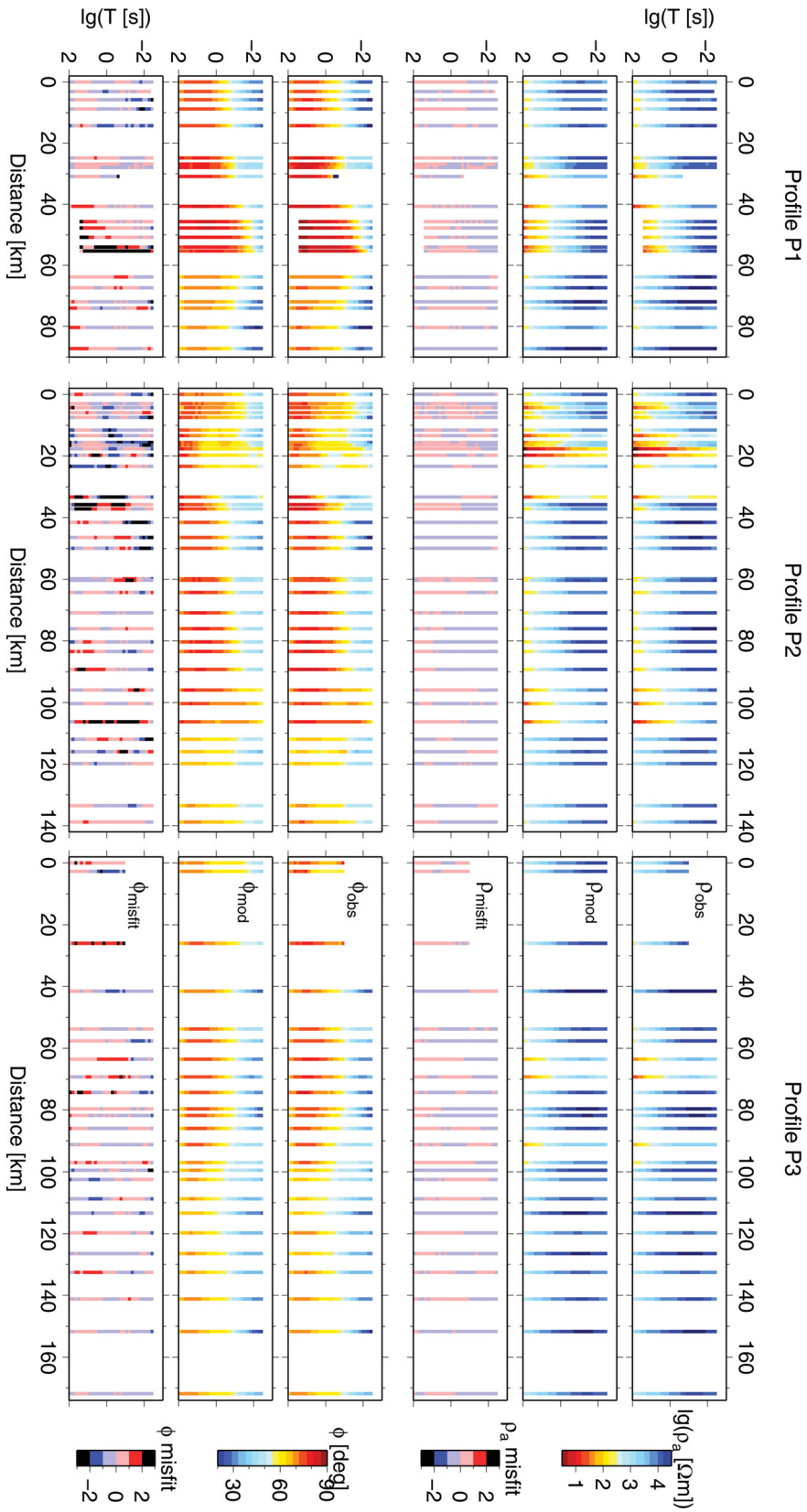

Figure 8. Pseudosections of observed (obs.) and model (mod.) responses and their misfits for each profile P1, P2 and P3. Each column represents one site. Misfits are normalized by data errors or error-floor in case it is larger than actual error. Apparent resistivities ρ_{obs}, ρ_{mod} and ρ_{misfit} in the three upper rows and impedance phases φ_{obs}, φ_{mod} and φ_{misfit} in the three lower rows. Note that the distances in this figure are depicted from the first sounding at 0 km for each profile, but in the following model plots the profiles P1 and P3 are shifted to the east.

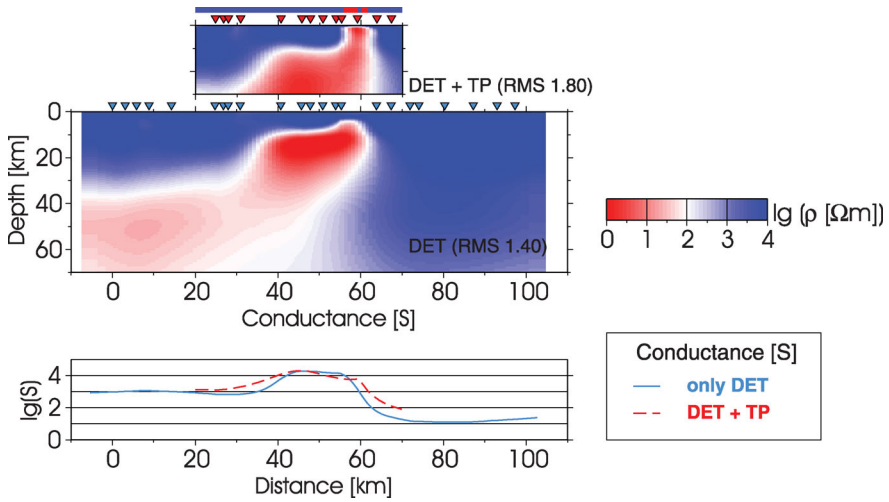

Figure 9. The effect of using the tipper (TP) in the inversion. The lower panel shows the final model from determinant (phase and apparent resistivity) inversion. The differing part from joint inversion test is shown in the small panel above. Conductances for each model calculated for the uppermost 70 km are drawn in the graph below. Site locations are marked with inverted triangles, and they are the same for both data sets except for one additional site (only tipper data) on top of KB for joint inversion.

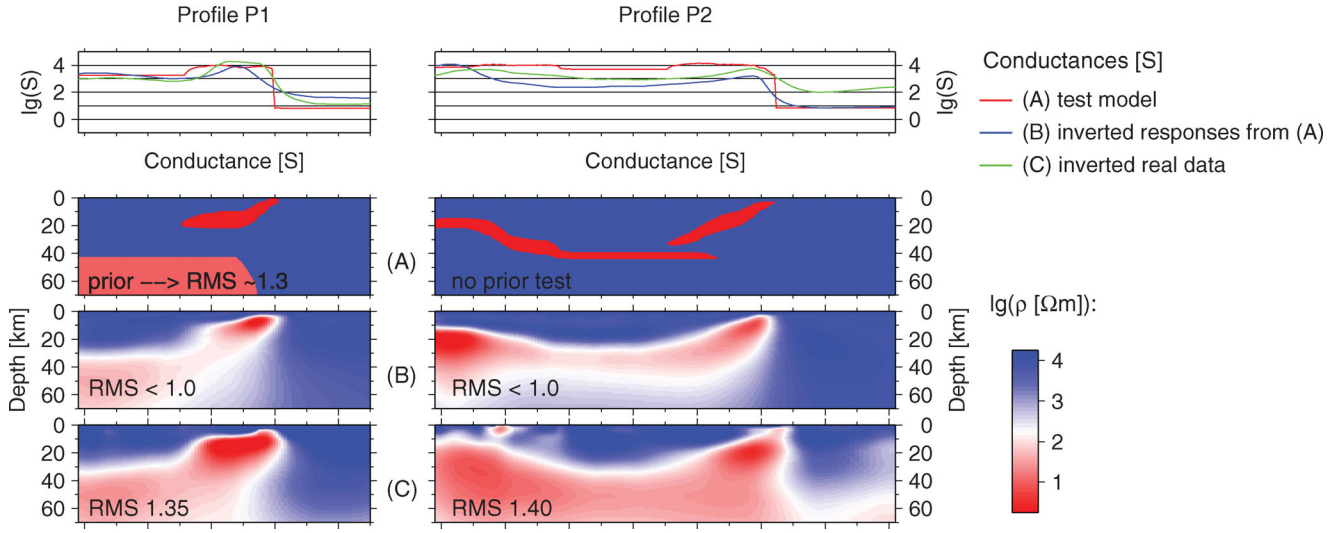

Figure 10. Resolution tests of the obtained models. Simplified alternative models (A) for the profiles were derived from the final inversion models (Fig. 7), which are redrawn in the lower panels (C) for comparison. Other geophysical information (reflection seismic models) was taken into account when the simplified models were created. Responses from simplified models were used as data for resolution analysis. Real errors were attached to synthetic responses, which were inverted to find the features that can be recovered. Results of these inversions are shown in the middle panel (B). Using the alternative models (A) as prior models the observed data could be inverted to roughly the same rms fit as the final inversion models, meaning that this kind of model can explain the measured data as well as the smooth models.

unrealistic model with clear artefacts. In conjunction with prior model tests described earlier, the sensitivity of the alternative models were tested by inverting their synthetic responses with the same data errors and same frequency and site distribution as in the observed data. One selected example for both P1 and P2 is shown in Fig. 10 (panel A). The results of the inversion of synthetic data are shown in Fig. 10 (panel B). The comparison of the synthetic inversion model with the original unconstrained inversion model (Fig. 10, panel C) indicates if the model (A) is among the geophysically acceptable models. Moreover, the comparison of the models (A) and (B) indicates which features can be recovered in the inversion process. This kind of synthetic testing answers for example on the questions of the penetration depth under the proposed structures.

The physics of EM methods and therefore natural application of Occam's type of inversion gives smooth models as a result. Those smooth models might not be easy to interpret in geological terms, since the real boundaries for different units tend to be sharper. The alternative models used in prior model testing were created by modifying the final inversion results, while considering the results from seismic reflection studies as well as geological background information. For example, the conductor A is replaced for model testing with a thinner layered conductor having a same conductance as in the original thick model. Using this kind of layered-type conductor (Fig. 10) in the prior model for the inversion, it is possible to get a result that fits the data equally well as the final smooth model shown in Figs 7 and 10.

Besides the conductor A, the properties of the conductors E, D1 and D2 and their relations to A were studied using prior models and synthetic testing. These tests in the profile P1 revealed that right under the conductor A1 the model resolution is very poor.

This was expected, since in the middle of this conductor, the data were restricted to 10 s. However, as there are data in the resistive areas to the east and west of the conductor, there is some resolution under its edges. Therefore the lower crustal conductor D1 should continue to the east under the conductor A, although it is uncertain how far to the east. Under the western edge of the conductor A, a thicker conductor or another conductor below A is required to produce the type of model seen in Fig. 7. A test model with only a single conductor A (10 km thick, 10 000 S conductance) in an otherwise resistive environment clearly produces resistive material below it although the data from the sites right above the conductor cannot penetrate through it. Model structure and properties in the profile P2 are similar to P1, and according to our dimensionality analysis this area is mostly 2-D, therefore it is assumed that also D2 can continue under A2. The top of the conductor D1 (and thus, most likely also D2) is not solved properly in the inversion of synthetic test data. This is seen for P1 comparing the models (A) and (B) in Fig. 10, where the top of D1 is below 40 km and at about 35 km, respectively. According to synthetic tests, this is due to the high contrasts in model resistivities (10 Ωm/10 000 Ωm). With lower contrast, the top is better resolved. As the top is at the same depth in both inversion models (B) and (C), the real structure is most likely also below 40 km as seen in (A).

Conductor E in P2 was also replaced with a thin layer for testing. Several models were used for the tests. In one set, the thin E conductor was a short conductor in the western part of the profile whereas in the other set, the thin elongated E conductor extends from the western end of the profile under A in the east. This alternative combines the conductors E and D2 (Fig. 7) into a single one (E-D2). The models had also either resistive or conductive lower crust (for the model of conductive lower crust, see the simplified model of P1 in Fig. 10). For the profile P2, a model with a long E conductor and resistive lower crust, is shown in Fig. 10 (panel A) together with the inversion result of that model (panel B) and the original unconstrained inversion model (panel C). In the case of a thin (<10 km) and continuous E-D2 with the conductance of 1000–8000 S, the synthetic model tests suggest a penetration through the conductor (Fig. 10, panel B). However, as seen in Fig. 7 and panel C in Fig. 10, in the model of P2, the whole western middle and lower crust is conductive. This indicates that conductive material is needed below the thin conductor E-D2. For example, a thicker conductor E-D2 or conductive lower crust to the west of the KB could solve the problem of missing conductive material. Another possible model geometry for P2 is a shorter thin conductor E that dips to about 40 km and a continuous lower crustal conductor D2 (below 40 km) underneath both E and A. In the final inversion model it is impossible to distinguish overlaying conductors E and D2 in the west, but together they can produce the observed inversion model. Furthermore, the strongest 3-D effects according to *Q*-function analysis are found at 20–40 km in P2, possibly indicating that the conductor E is local and explaining why E is not seen at P3. The different nature of the conductors A and E is already observed in the data (Fig. 8)—in the case of E the phases grow higher slowly and steadily over the periods (P2 first 20 km), whereas in the case of A they rise fast (P1 40–60 km).

In the relatively homogenous profile P3, a small deep conductive formation (K) was detected in the middle of the profile. This conductor is needed to fit the data. To find constraints for the interpretation, several models with simple geometries that would support different hypotheses on the origin of the conductor (vertical, east/westward dipping plates) were tested. The best fit is obtained with a horizontal plate model, but all other tested geometries also provide a better fit than the original smooth conductor. The western part of P3 (J) would be consistent with the idea of conductive lower crust (D1 and D2) in the models for P1 and P2. According to prior testing, a model with moderately conducting lower crust explains the data. However, the conductivity of J should be clearly lower (max 100 Ωm) than in D1 and D2 (10 Ωm). Also the top of J should be deeper than D1 and D2.

Other features tested with prior models are the conductors H1–H3 and F (Fig. 7). The results of the synthetic tests (not shown in the paper) suggest that the conductors H1–H3 are rather unstable features and possibly artefacts. Inverting of responses from models with extremely conductive slab A where eastern crust is totally resistive occasionally results in similar lower crustal conductors in the eastern part of the profile. On the other hand, in prior model tests, where resistive Archaean crust is set at 10 000 Ωm, the inversion of measured data systematically creates the conductors H1–H3. Thus a part of the conductivity in the eastern edges is probably due to lateral effects from A, but slightly conductive material H in the east is probably needed to fit the data. It would be interesting to continue the profiles to the east to verify the presence of these conductors, but as they are mostly in the depth of upper mantle already they are not the main concern of this study. The near-surface conductor F is observed in the profile P2 and can be seen in the airborne EM maps (Fig. 1b). The tests of the downward continuation and a possible connection of F with the crustal conductor E revealed that F and E are most likely the separate conductors.

5 GEOLOGICAL INTERPRETATION AND DISCUSSION

The interpretation based on conductivity models and FIRE reflection seismic model (Fig. 11) is shown in Fig. 12 and is discussed later. Note that for profile P2, two alternative interpretations are given (the two middle panels in Fig. 12). The conductors A1 and A2 can be replaced by thinner layered-type conductors as shown in Fig. 10. A few kilometres thick moderately conducting layer is equivalent to a resistive layer hosting several very thin highly conductive sheets as long as the total conductance is the same. In the thin conductor model, resistivity of 1 Ωm and thickness of 10 km are used for A, which gives the total conductance of 10 000 S. The same conductance can be achieved with a layer having a thickness of 5 km and resistivity of 0.5 Ωm. This kind of stacks of alternating resistive and conductive sheets with graphite are found in the Lapland Granulite Belt (Korja *et al.* 1996). Good near-surface conductors in the KB area are clearly seen on AEM maps (Fig. 1c). Geological mapping has shown that the near-surface conductors are caused by graphite and/or sulphide-bearing metasedimentary rocks. In the Outokumpu Area, Rekola & Ahokas (1987), for example, identified several very thin black schist layers in drill holes at the depth of about 1 km. The thickest layer has a thickness of 77 m and resistivity of 0.01 Ωm yielding 7700 S for total conductance.

The conductors A1 and A2 are interpreted as a stack of graphite-bearing metasedimentary rocks of the KB dipping from the east under the Archaean RC and IC, represented by upper crustal resistive units C1, C2 and C3. The enigmatic conductor below IC (K in P3; Figs 7 and 12) could represent an unexposed southwestern continuation of the stack. The 2-D models show the dip angles of about 20° on P1 and closer to about 45° on P2 indicating lateral changes in the geometry of the KB and IC above it. According to the interpretation of the FIRE reflection seismic data, the underthrust SB cuts the westward dipping KB and obviously marks also

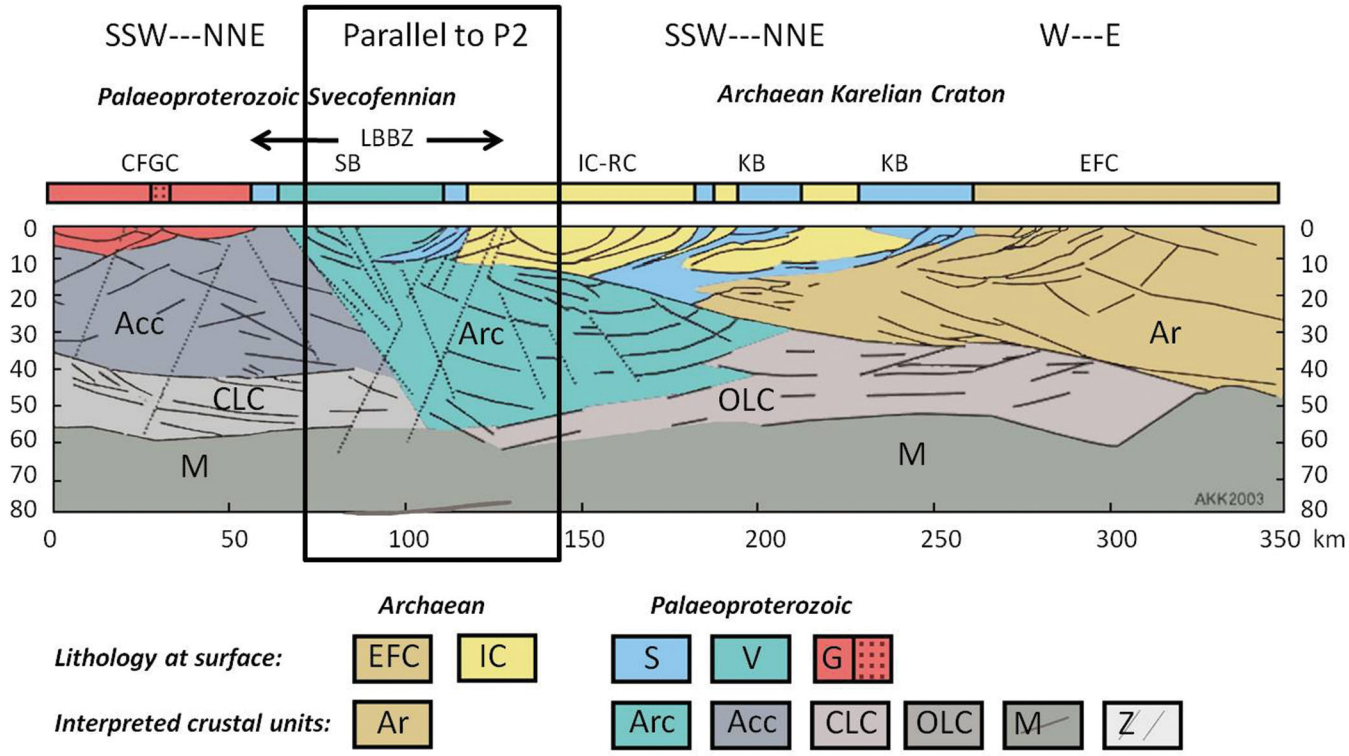

Figure 11. Geological interpretation of the reflection seismic FIRE-1 line for the eastern part of the line redrawn from Lahtinen *et al.* (2009). The area where the FIRE-1 is parallel to our profile P2 is outlined with a black box. Appreviations: Lithological units: Ar, Archaean rocks in the Eastern Finland (EFC), Iisalmi (IC) and Rautavaara (RC) Complexes; S, sedimentary rocks in the Kainuu (KB) and Savo (SB) Belts; V, volcanic and sedimentary rocks on the Savo Belt (SB); G, Calc-alkaline/subalkaline granitoids in the Central Finland Granitoid Complex (CFGC). Interpreted units: Ar, Archaean crust; Arc, arc rocks; Acc, accreted material; CLC, granulitic lower crust (continental); OCL, granulitic lower crust (oceanic); M, upper-mantle rocks with reflections in refraction data; Z, shear zones; LBBZ, Lake Ladoga – Bothnian Bay zone.

the bottom of the IC (Lahtinen *et al.* 2009). Consequently, the depth of the KB conductors define the maximum thickness of the IC (see Fig. 12). The interpreted thickness of the IC in P1 (15 km) is compatible with the FIRE interpretation. According to our results, the IC is thickening in P2 to 25 km.

The resistive features C1–C3 are considerably thicker than the interpreted thickness of the IC, indicating, that the upper part of the SB is also mostly resistive and not distinguishable electrically from the Archaean IC. However, prominent conductors (E, F and D1, D2) are found within the SB. Likewise the conductor A, the conductor E is also interpreted as a stack of alternating highly conductive and more resistive metasediments (Figs 10 and 12). This stack dips eastwards approximately to the depth of 40 km under the lithological border between SB and IC. Two possible interpretations for the geometry of E are given in Fig. 12 (P2-a and P2-b). In the first model, E continues to the east under the KB. In this model, middle crustal E and lower crustal D2 together explain the enhanced conductivity in the central part of the profile P2. In the second model, E is confined to the western part of the SB and D2 represents solely the enhanced conductivity mentioned earlier. The near-surface conductors in the western part of P2 (conductors F) represent a shallow formation of metasediments not connected to the larger and deeper conductor E.

The conductor D2 seems to continue to the west under E, possibly crossing the lower crustal boundary between the SB and the Keitele microcontinent (Fig. 11). Thus the enhanced conductivity is not related only to SB lithologies. It was found out during inversion testing that these conductive rocks may continue eastwards under the KB, which is consistent with the FIRE-1 interpretation. At P3, the lower crust is not as conductive as at P1 and P2. However, the observed enhanced lower crustal conductivity J might be related to D1 and D2. Especially in the case of interpreted conductor E continuing far to the east and under KB, the whole conductor D can be explained as the superposition of J and E (Fig. 12).

The conductive Proterozoic lower crust has previously been observed in the GGT/SVEKA profile (Korja & Koivukoski 1994; Lahti *et al.* 2002). The possible causes of enhanced lower crustal conductivity in stable shield areas such as Fennoscandia are widely discussed (e.g. Jones 1992; Korja *et al.* 1996), and include mineralogy, graphite and fluids. According to Moisio & Kaikkonen (2001), the suggested lower crustal high conductive layer could be connected to rheologically very weak layer, provided the lower crust is wet or the strain rate is low enough. However, fluids are highly implausible explanation for enhanced lower crustal conductivity on very old stable areas as they would require long retention time unless a continuous recharge can be provided. Instead, interconnected graphite films from an organic or inorganic source provide a more likely conductivity mechanism (see references e.g. in Korja *et al.* 1996). A comparison of P3 with FIRE-1 geological interpretation suggests that the feature J is connected to granulitic lower crust of the Keitele microcontinent (Figs 11 and 12). Consequently, the granulite facies metamorphosis, that is, CO_2 from the mantle (e.g. Newton *et al.* 1980), might explain the presence of conductive graphite in the lower crust. Alternatively, the carbon

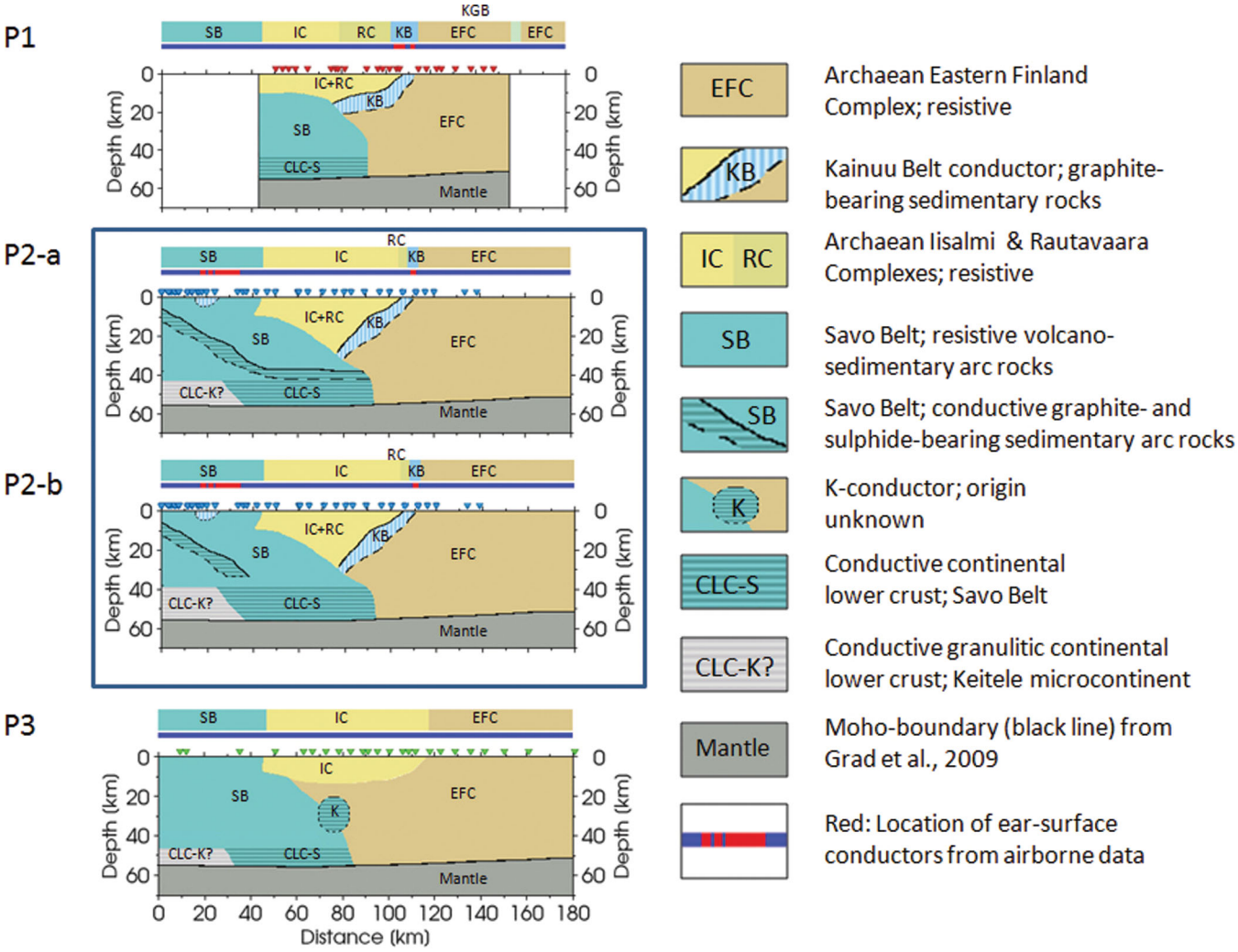

Figure 12. Schematic geological interpretation for profiles P1–P3, based on interpretative models discussed in Sections 4 and 5. Certain features that cannot be distinguished with MT (such as the boundary between two resistive units IC and SB) are modified from the interpretation of FIRE-1 (Lahtinen *et al.* 2009). The most accurately resolved features in our models are the tops of the conductive metasedimentary rocks: they are marked with black lines. Two possible structures for P2 are proposed based on different relative geometries of the conductors E and D2 (Fig. 7). The lower boundary of the highly conductive metasedimentay rocks is drawn as a dashed line denoting that the most uncertain parts of the model are beneath the conductors. The other features presented below the metasedimentary rocks—SB-EFC boundary and CLC-K—are also uncertain due to reduced resolution. Moho depth taken from Grad *et al*. (2009).

could have originated from sedimentary source, as suggested by Korja *et al.* (1996) for the origin of the carbon in Lapland Granulite Belt.

According to our models (B1–B3 in Fig. 7) the resistivities of the entire Archaean crust range from a few thousands of ohm metres to tens of thousands of ohm metres. The resistive Archaean material from EFC most likely continues under the conductors of KB (Figs 10 and 12), as also suggested by the FIRE-1 geological interpretation (Lahtinen *et al.* 2009). The faint conductor I coincides with a major fault zone between the IC and the EFC. As seen in Figs 1(b) and (c), the strike of the fault zone is in general perpendicular to our profile, but the zone makes a curve where profile P3 crosses it. This likely explains why it is seen as a wider conductive area in the model.

6 CONCLUSIONS

Based on the results of 2-D inversions from three MT profiles across the Archaean–Proterozoic boundary zone, the following conclusions on the conductivity structure are drawn:

The conductors related to the Proterozoic KB and SB were formed on the surface and transported to deeper crustal levels in the collision of the Karelian Craton and Keitele microcontinent (Savo orogeny). They form a bowl-shaped structure under the resistive Archaean IC and RC.

Electrically the SB is heterogeneous. It is composed of highly resistive and highly conductive blocks. The eastward dipping conductors of the SB are located in the lower parts of the formation and extend to the east possibly cutting the westward dipping KB, which is flanked above and below by the Archaean IC/RC and EFC.

There are no prominent crustal conductors between the KB and the Outokumpu Area to the south. The moderately conducting feature between these areas most likely represents the shear zones between the Archaean IC/RC and EFC.

The crust in the Karelian craton is highly resistive having only minor resistivity variations in our research area. In particular, also the Archaean lower crust is resistive on the contrary to the conductive lower crust of the Proterozoic SB (granulitic lower crust of the Keitele microcontinent).

ACKNOWLEDGMENTS

NordForsk mobility stipend granted to KV made possible a few months visit in Uppsala, where Prof. Laust B. Pedersen provided useful insight, ideas and feedback on the early stages of the inversion and analysis of the data. We also acknowledge Prof. Lauri Lajunen, the rector of the University of Oulu for the special instrument grant awarded to bring our field equipment up-to-date. We also wish to thank Minna Löytynoja, Mikko Mali, Hanna Silvennoinen and Kalle Suvanto, geophysics students, who have participated in the field work during summers 2003–2005. Martyn Unsworth, the editor and Laszlo Szarka and Juanjo Ledo, provided a thorough review and helpful comments and suggestions that led to the improvement of the manuscript. The project was funded by the Academy of Finland through the project no 201548.

REFERENCES

Ádám, A., Kaikkonen, P., Hjelt, S.E., Pajunpää, K., Szarka, L., Verö, J. & Wallner, A., 1982. Magnetotelluric and audiomagnetotelluric measurements in Finland, *Tectonophysics,* **90,** 77–90.

Airo, M.-L. (ed.), 2005. Aerogeophysics in Finland 1972–2004: Methods, System Characteristics and Applications. Special Paper 39, 197 pages, 115 figures, 12 table and 8 appendices, Geological Survey of Finland.

Bahr, K., 1988. Interpretation of the magnetotelluric impedance tensor: regional induction and local telluric distortion, *J. Geophys.,* **62,** 119–127.

Bahr, K., 1991. Geological noise in magnetotelluric data: classification of distortion types, *Phys. Earth planet. Inter.,* **66,** 24–38.

Berdichevsky, M.N. & Dmitriev, V.I., 1976. Basic principles of interpretation of magnetotelluric sounding curves, in *Geoelectric and Geothermal Studies,* pp. 165–221, ed. Ádám, A., KAPG Geophysical Monograph, Akadémiai Kiadó.

Berdichevsky, M.N. & Dmitriev, V.I., 2009. Models and methods of magnetotellurics, *Scientific World,* Moscow, Russia, 680 p. (in Russian).

Berdichevsky, M.N. & Pokhotelov, D.O., 1997. Violation of the dispersion relations in a three-dimensional magnetotelluric model, *Izvestiya, Phys. Solid Earth,* **8**(33), 603–612.

Cagniard, L., 1953. Basic theory of the magneto-telluric method of geophysical prospecting, *Geophysics,* **18,** 605–635.

Duba, A., Heikamp, S., Meurer, W., Nover, G. & Will, G., 1994. Evidence from borehole samples for the role of accessory mineral in lower-crustal conductivity, *Nature,* **367,** 59–61.

Gaál, G. & Gorbatschev, R., 1987. An outline of the Precambrian evolution of the Baltic Shield, *Precambrian Res.,* **35,** 15–52.

Gorbatschev, R. & Bogdanova, S., 1993. Frontiers in the Baltic Shield, *Precambrian Res.,* **64,** 3–21.

Grad, M., Tiira, T. & ESC Working Group, 2009. The Moho depth map of the European Plate, *Geophys. J. Int.,* **176,** 279–292, doi:10.1111/j.1365-246X.2008.03919.x.

Hjelt, S.-E., Korja, T., Kozlovskaya, E., Lahti, I., Yliniemi, J., BEAR, SVEKALAPKO Seismic Tomography Working Groups (2006). Electrical conductivity and seismic velocity structures of the lithosphere beneath the Fennoscandian Shield, in *European Lithosphere Dynamics,* pp. 541–559, eds Gee, D.G. & Stephenson, R.A., Geological Society, London, Memoirs 32.

Jones, A.G., 1992. Electrical conductivity of the continental lower crust, in *The Lower Continental Crust,* pp. 81–143, eds Fountain, D.M., Arculus, R.J. & Kay, R.W., Elsevier, Amsterdam, The Netherlands.

Jones, A.G., 1998. Waves of the future: superior inferences from collocated seismic and electromagnetic experiments, *Tectonophysics,* **286,** 273–298.

Kaikkonen, P. & Pajunpää, K., 1984. Audiomagnetotelluric measurements across the Lake Ladoga-Bothnian Bay zone in central Finland, *Geophys. J. R. astr. Soc.,* **78,** 439–452.

Koistinen, T., Stephens, M.B., Bogatchev, V., Nordgulen, Ø., Wennerström, M. & Korhonen J., 2001. *Geological Map of the Fennoscandian Shield, Scale 1:2 000 000,* Geological Survey of Finland, Espoo; Geological Survey of Norway, Trondheim; Geological Survey of Sweden, Uppsala; North-West Department of Natural Resources of Russia, Moscow.

Kontinen, A. & Meriläinen, K., 1993. *Paltamo. Geological Map of Finland 1:100000: Pre-Quaternary Rocks, Sheet 3434*. Geological Survey of Finland, Espoo.

Korja, T., 1993. Electrical conductivity distribution of the lithosphere in the Central Fennoscandian Shield, *Precambrian Res.,* **64,** 85–108.

Korja, T. & Hjelt, S.-E., 1998. The Fennoscandian Shield: a treasury box for deep electromagnetic studies, in *Deep Electromagnetic Exploration,* pp. 31–73, eds Roy, K.K., Verma, S.K. & Mallick, K., Narossa Publishing House, New Delhi, India.

Korja, T. & Koivukoski, K., 1994. Magnetotelluric investigations along the SVEKA profile in central Fennoscandian Shield, Finland, *Geophys. J. Int.,* **116,** 173–197.

Korja, A., Korja, T., Luosto, U & Heikkinen, P., 1993. Seismic and geoelectric evidence for collisional and extensional events in the Fennoscandian Shield: implications for Precambrian crustal evolution, *Tectonophysics,* **219,** 129–152.

Korja, T., Tuisku, P., Pernu, T. & Karhu, J., 1996. Lapland Granulite Belt: implications for properties and evolution of deep continental crust, *Terra Nova,* **8,** 48–58.

Korja, A., Lahtinen, R. & Nironen, M., 2006. The Svecofennian orogen: a collage of microcontinents and island arcs, in *European Lithosphere Dynamics,* pp. 561–578, eds Gee, D.G. & Stephenson R.A., Geological Society, London, Memoirs, 32.

Korsman, K., Koistinen, T., Kohonen, J., Wennervirta, M., Ekdahl, E., Honkamo, M., Idman, H. & Pekkala, Y. (ed.), 1997. *Suomen kallioperäkartta 1:1 000 000,* Geologian tutkimuskeskus, Espoo.

Korsman, K., Korja, T., Pajunen, M., Virransalo, P. & the GGT/SVEKA Working Group, 1999. The GGT/SVEKA Transect: structure and evolution of the continental crust in the palaeoproterozoic Svecofennian Orogen in Finland, *Int. Geol. Rev.,* **41**(4), 287–333.

Kukkonen, I.T & Lahtinen, R. (ed.), 2006. Finnish Reflection Experiment FIRE 2001–2005, Geological Survey of Finland, Special paper 43, 247 p.

Kukkonen, I. T., Heikkinen, P., Ekdahl, E., Hjelt, S-E., Yliniemi, J., Jalkanen, E. & FIRE Working Group, 2006. Acquisition and geophysical characteristics of reflection seismic data on FIRE transects, Fennoscandian Shield, in *Finnish Reflection Experiment FIRE 2001–2005,* pp. 13–43, eds Kukkonen, I.T. & Lahtinen, R., Geological Survey of Finland, Special Paper 43.

Lahti, I., Korja, T., Pedersen, L. B. & the BEAR Working Group, 2002. Lithospheric conductivity along GGT/SVEKA Transect: implications from the 2-D inversion of magnetotelluric data, in *Lithosphere 2002, Second Symposium on the Structure, Composition and Evolution of the Lithosphere in Finland,* pp. 75–78, eds Lahtinen, R., Korja, A., Eklund, O., Hjelt, S.E. & Pesonen, L.J., Institute of Seismology, University of Helsinki, Report S-42.

Lahtinen, R., 1994. Crustal evolution of the Svecofennian and Karelian Domains during 2.1–1.79 Ga, with special emphasis on the geochemistry and origin of 1.03–1.91 Ga gneissic tonalites and associated supracrustal rocks in the Rautalampi area, central Finland, *Geol. Surv. Finland Bull.*, **378,** 128.

Lahtinen, R., Huhma, H. & Kousa, J., 2002. Contrasting source components of the Palaeoproterozoic Svecofennian metasediments: detrital zircon U-Pb, Sm-Nd and geochemical data, *Precambrian Res.,* **116,** 81–109.

Lahtinen, R., Korja, A., Nironen, M. & Heikkinen, P., 2009. Palaeoproterozoic accretionary processes in Fennoscandia, in *Earth Accretionary Systems in Space and Time,* pp. 237–256, eds Cawood, P. A. & Kröner, A., Geological Society, London, Special Publications 2009, 318.

Ledo, J., Queralt, P., Marti, A. & Jones, A.G., 2002. Two-dimensional interpretation of three-dimensional magnetotelluric data: an example of limitations and resolution, *Geophys. J. Int.,* **150,** 127–139.

Luosto, U., 1991. Moho depth map of the Fennoscandian Shield based on seismic refraction data, in *Structure and Dynamics of the Fennoscandian Lithosphere, in Proceedings of the Second Workshop on Investigation of the Lithosphere in the Fennoscandian Shield by Seismological Methods,* Helsinki, May 14–18, 1990, pp. 43–49, Rep., S-25, ed. Korhonen, H. & Lipponen, A., Inst. Seismology, Univ. Helsinki.

Luosto, U., 1997. Structure of the Earth's crust in Fennoscandia as revealed from refraction and wide-angle reflection studies, in *The Lithosphere in Finland: A Geophysical Perspective,* pp. 3–16, ed. Pesonen, L.J., Geophysica, **33**: 1, Helsinki, Finland.

Luosto, U., Lanne, E., Korhonen, H., Guterch, A., Grad, M., Materzok, R. & Perchuc, E., 1984. Deep structure of the Earth's crust on the SVEKA profile in the Central Finland, *Ann. Geophys*., **2**(5), 559–570.

Luukkonen, E.J., 2001. Lentiiran kartta-alueen kallioperä. Summary: prequaternary rocks of the Lentiira map-sheet area, in *Geological Map of Finland 1:100000. Explanation to the Maps of Pre-Quarternary Rocks, Sheet 3321,* 51 p., Geological Survey of Finland, Espoo, Finland.

Moisio, K. & Kaikkonen, P., 2001. Geodynamics and rheology of the lithosphere along the DSS profile SVEKA in the central Fennoscandian Shield, *Tectonophysics,* **340,** 61–77.

Newton, R.C., Smith, J.V. & Winkley, B.F., 1980. Carbonic metamorphism, granlites and crustal growth, *Nature,* **288,** 45–50.

Nironen, M., 2003. Keski-Suomen granitoidikompleksi: karttaselitys. Summary: central Finland Granitoid Complex, explanation to a map, *Geologian tutkimuskeskus. Tutkimusraportti* **147,** 45 (in Finnish).

Nironen, M., Lahtinen, R. & Koistinen, T., 2002. Suomen geologiset paikannimet – yhtenäisempään nimikäytäntöön! Summary: subdivision of Finnish bedrock, and attempt to harmonize terminology, *Geologi,* **54,** 8–14 (in Finnish).

Paavola, J., 1990. *Iisalmi. Geological Map of Finland 1:100 000: Pre-Quaternary Rocks, Sheet 3342,* Geological Survey of Finland, Espoo.

Paavola, J., 1999. Rautavaaran kartta-alueen kallioperä. Summary: prequaternary rocks of the Rautavaara Map-Sheet Area. Geoogical map of Finland 1:100 000. Explanation to the maps of pre-quaternary rocks, sheet 3343, *Geological Survey of Finland,* 53 p. (in Finnish).

Pajunpää. K., 1984. Magnetometer array studies in Finland: determination of single station transfer functions, *J. Geophys.,* **55,** 153–160.

Pajunpää, K., 1987. Conductivity anomalies in the Baltic Shield in Finland, *Geophys. J. R. astr. Soc.,* **91,** 657–666.

Parkinson, W.D., 1962. The influence of continents and oceans on geomagnetic variations, *Geophys. J.,* **2,** 441–449.

Pedersen, L.B. & Engels, M., 2005. Routine 2D inversion of magnetotelluric data using the determinant of the impedance tensor, *Geophysics,* **70**(2), G33–G41, doi:10.1190/1.1897032.

Peltoniemi, M., Korhonen, J. & Hjelt, S.-E. 1990. Electrical conductance of the surficial parts of the crust (0 – 150 m) as interpreted from airborne survey data, Map 29a, in *Atlas of Finland, Appendix 123–126 (1990) Geology,* 5th edn, ed. Alalammi, P., National Board of Survey, Helsinki, Finland.

Pirttijärvi, M., 1995. TRANSAEM, Fortran-77 ohjelma GTK:n sähkömagneettisen lentomittausaineiston muuntamiseksi näennäiseksi johtavuudeksi ja syvyydeksi, *Geological Survey of Finland,* Internal Report Q17.9/95/1 (in Finnish).

Rekola, T. & Ahokas, T. 1987. Findings from geophysical surveys in the Outokumpu zone, Finland, *Paper Presented in the 49th Annual Meeting and Technical Exhibition*, EAEG, 8–12 June 1987, Belgrad, 15 p.

Siripunvaraporn W. & Egbert, G. 2000. An efficient data-subspace inversion for two dimensional magnetotelluric data, *Geophysics,* **65,** 791–803.

Smirnov, M.Yu., 2003. Magnetotelluric data processing with a robust statistical procedure having a high breakdown point, *Geophys. J. Int.,* **152,** 1–7.

Smirnov, M.Y. & Pedersen, L.B., 2009. Magnetotelluric measurements across Sorgenfrei-Tornquist zone in southern Sweden and Denmark, *Geophys. J. Int.,* **176,** 443–456.

Smirnov, M., Korja, T., Dynesius, L., Pedersen, L.B. & Laukkanen, E. 2008. Broadband magnetotelluric instruments for near-surface and lithospheric studies of electrical conductivity: a Fennoscandian pool of magnetotelluric instruments, *Geophysica,* **44**(1–2), 31–44.

Stålhös, G., 1976. Aspects of the regional tectonics of eastern central Sweden, *Geologiska Föreningens i Stockholm Förhandlongar,* **98,** 146–154.

Suominen, V., 1991. The Chronostratigraphy of Southwestern Finland, with Special Reference to Postjotnian and Subjotnian Diabases, Geologica Survey of Finland, Bulletin, 356.

Tikhonov, A.N., 1950. Determination of the electrical characteristics of the deep strata of the Earth's Crust, *Dok. Akad. Naut., USSR*, **73,** 295–297.

Weidelt, P. & Kaikkonen, P., 1994. Local 1-D interpretation of magnetotelluric B-polarization impedances, *Geophys. J. Int.,* **117,** 733–748.

Wiese, H., 1962. Geomagnetische Tiefentellurik Teil II: die Streichrichtung der Untergrundstrukturen des elektrischen Widerstandes, erschlossen aus geomagnetischen Variationen, *Geofisica Pura e Applicata,* **52,** 83–103.

Zhang, P., Roberts, R.G. & Pedersen, L.B., 1987. Magnetotelluric strike rules, *Geophysics,* **52,** 267–278.